Bulletin of the Seismological Society of America. Vol. 66, No. 5, pp. 1539–1554. October 1976

BODY WAVES IN A LAYERED ANELASTIC SOLID

By W. Silva

ABSTRACT

A formulation extending the Haskell-Thompson matrix method to include the effects of anelastic attenuation is presented. The formulation is exact in that no low-loss approximations are made. Consideration is given to nonparallel propagation and attenuation directions with corresponding velocity anisotropy. Examples are presented for models representing soils, the crust, and the core-mantle boundary.

Introduction

With the increase in the number of stations and the higher degree of standardization in recent years, more use is being made of seismic amplitude data. This has contributed to an increased regionalization of structure down to the core-mantle boundary. In order to accurately represent this fine structure in applying corrections or to resolve it in inverting data, more use is being made of the higher frequencies where the attenuation effects are most significant. It is therefore becoming increasingly important to consider nongeometrical attenuation exactly. Past approximations in dealing with loss (Knopoff, 1964) must be replaced with exact formulations (Lockett, 1962; Cooper, 1967; Borcherdt, 1971; Buchen, 1971).

In order to consider the effects of a vertical variation in attenuation as well as velocity and density on body waves, an extension of the Haskell-Thompson (Haskell, 1953) matrix formulation using an exact theory is presented. In particular, the restricted problem of anelastic layers on an elastic half-space is considered, but the formulation can easily be extended to include an attenuating half-space. Previous consideration of the problem (Kanai, 1950) dealt with normally incident homogeneous waves with viscoelasticity of the Voigt type. The present treatment considers incident P or SV waves at arbitrary angles and a general constitutive relation.

Formulation

The most general form of a linear constitutive relation is Boltzman's superposition principle (Gurtin and Sternberg, 1962) which, written in terms of the tensorial relaxation function $r(t)$ is

$$\begin{aligned} P_{ij}(t) &= \int_{-\infty}^{t} r_{ijkl}(t-\tau)\, d\varepsilon_{kl}(\tau) \\ &= r_{ijkl}(t) * d\varepsilon_{kl}(t) \end{aligned} \tag{1}$$

where $P_{ij}(t)$ and $\varepsilon_{ij}(t)$ are the time-dependent stress and strain tensors and the symbol $*$ denotes the Stieltjes convolution.

Assuming the medium to be isotropic and homogeneous, equation (1) may be broken up into bulk and shear components and written as

$$\begin{aligned} P_{ij}(t) &= 2\mu(t) * d\varepsilon_{ij}(t) \qquad i \neq j \\ P_{kk}(t) &= 3\kappa(t) * d\varepsilon_{kk}(t) \end{aligned} \tag{2}$$

where $\mu(t)$ and $\kappa(t)$ are the relaxation functions in shear and bulk. Assuming that the

particle displacements u_i are infinitesimal, the strain can be written

$$\varepsilon_{ij}=\tfrac{1}{2}[u_{i,j}+u_{j,i}]$$

and, neglecting body forces, the linear momentum equation is

$$P_{ij,j}(t)=\rho\ddot{u}_i \tag{3}$$

where ρ is the medium density. Substituting equation (2) into equation (3) yields the equation of motion.

$$[\kappa(t)+\tfrac{4}{3}\mu(t)]*[\nabla(\nabla\cdot d\mathbf{u})]-[\mu(t)*[\nabla\times(\nabla\times d\mathbf{u})]=\rho\ddot{\mathbf{u}}. \tag{4}$$

Since the convolutions make the time-domain representation quite intractable, it is customary to take the Fourier transform of equation (4). Restated in terms of transformed variables, equation (4) becomes

$$[\bar{\kappa}+\tfrac{4}{3}\bar{\mu}]\nabla(\nabla\cdot\bar{\mathbf{u}})-[\bar{\mu}]\nabla\times(\nabla\times\bar{\mathbf{u}})=-\rho\omega^2\bar{\mathbf{u}} \tag{5}$$

where

$$\bar{\kappa}=i\omega\textstyle\int_{-\gamma}^{\infty}\kappa(t)e^{-i\omega t}\,dt, \qquad \bar{\mu}=i\omega\int_{-\alpha}^{\infty}\mu(t)e^{-i\omega t}\,dt$$
$$\bar{\mathbf{u}}=\textstyle\int_{-\infty}^{\infty}\mathbf{u}e^{i\omega t}\,dt.$$

At this point it is convenient to introduce the transformed P and S displacement potentials in terms of Helmholtz's relation

$$\bar{\mathbf{u}}=\nabla\bar{\phi}+\nabla\times\bar{\psi}, \qquad \nabla\cdot\bar{\psi}\equiv 0. \tag{6}$$

Substituting equation (6) into equation (5) results in the familiar Helmholtz equations for the P and S potentials $\bar{\phi}$ and $\bar{\psi}$.

$$[\nabla^2+K_P{}^2]\bar{\phi}=0, \qquad [\nabla^2+K_S{}^2]\bar{\psi}=0 \tag{7}$$

where

$$K_P{}^2=\frac{\omega^2}{\bar{\alpha}^2}=\omega^2\frac{\rho}{\bar{\kappa}(\omega)+\frac{4}{3}\bar{\mu}(\omega)}$$
$$K_S{}^2=\frac{\omega^2}{\bar{\beta}^2}=\omega^2\frac{\rho}{\bar{\mu}(\omega)}. \tag{8}$$

Note that the terms $\bar{\alpha}^2$ and $\bar{\beta}^2$ are in general frequency-dependent in both real and imaginary parts.

Medium Parameterization

Let us now consider, for demonstration purposes, the case of S waves. A general solution for $\bar{\psi}$ in equation (7) is

$$\bar{\psi}=\bar{\psi}(\omega)\exp(-i\mathbf{K}_S\cdot\mathbf{X}) \tag{9}$$

where $\mathbf{K}_S$ is a complex vector with the real and imaginary parts having different directions in general.

$$\mathbf{K}_S=\mathbf{P}_S-i\mathbf{A}_S \tag{10}$$

$$K_S{}^2=\mathbf{K}_S\cdot\mathbf{K}_S=|P_S|^2-|A_S|^2-i2\mathbf{P}_S\cdot\mathbf{A}_S \tag{11}$$

$$\mathbf{P}_S\cdot\mathbf{A}_S=|\mathbf{P}_S|\,|\mathbf{A}_S|\cos(\gamma_S). \tag{12}$$

$\mathbf{P}_S$ is the propagation vector such that $\omega/|\mathbf{P}_S|$ is the phase velocity and $\mathbf{A}_S$ the attenuation vector such that $\exp(-\mathbf{A}_S \cdot \mathbf{X})$ represents the spatial decay of the potential. The nonzero γ_s gives rise to the inhomogeneous waves (Borcherdt 1971, Buchen 1971, Cooper 1967, Lockett 1962) whose amplitude varies (monotonically) along a wave front. It becomes necessary now to specify the three parameters $|\mathbf{P}_S|$, $|\mathbf{A}_S|$, and γ_s in terms of material properties and medium geometry.

Writing the transformed shear modulus $\bar{\mu}(\omega)$ in equation (8) in terms of a real part, $\bar{\mu}_R(\omega)$, and an imaginary part, $\bar{\mu}_I(\omega)$, the quality factor Q_S for shear waves is defined as

$$Q_S^{-1} = \frac{\bar{\mu}_I(\omega)}{\bar{\mu}_R(\omega)} = \frac{1}{2\pi}\frac{\Delta E}{E} \tag{13}$$

where E is the peak energy density stored and ΔE is the energy lost, both per cycle (Borcherdt, 1971, 1973). K_S^2 may be written in the following form

$$K_S^2 = \frac{\omega^2}{v_s^2}\frac{2}{1+\sqrt{1+Q_S^{-2}}}\left(1-\frac{i}{Q_S}\right) \tag{14}$$

where v_s is the homogeneous wave velocity of the medium. Using (14) to invert (11) and (12) we arrive at convenient expressions for $|\mathbf{P}_S|$ and $|\mathbf{A}_S|$

$$|\mathbf{P}_S|^2 = \frac{\omega^2}{v_s^2}\frac{1}{1+\sqrt{1+Q_S^{-2}}}\left(1+\sqrt{1+Q_S^{-2}\cos^{-2}(\gamma_s)}\right) \tag{15}$$

$$|\mathbf{A}_S|^2 = \frac{\omega^2}{v_s^2}\frac{1}{1+\sqrt{1+Q_S^{-2}}}\left(-1+\sqrt{1+Q_S^{-2}\cos^{-2}(\gamma_s)}\right) \tag{16}$$

with similar expressions for P waves using the P parameters. In the low-loss approximation for homogeneous waves ($\gamma_s = 0$, $Q_s \gg 1$) equation (16) reduces to the well-known expression

$$|\mathbf{A}| = \frac{\omega}{2v_s Q_S}.$$

When dealing with highly dissipative materials the vectorial nature of $\mathbf{A}$ must be considered. The problem is that for a given incident wave (direction of both $\mathbf{P}$ and $\mathbf{A}$ specified) onto a plane boundary between two viscoelastic media, the direction of both P and A must be determined for the P and SV reflected and transmitted waves. These directions can be uniquely determined by applying the usual boundary conditions at a welded interface (or free surface for half-space problems). This results in an extended form of Snell's law in that A_x as well as P_x must be continuous (Borcherdt 1973, Lockett 1962). In the restricted case considered in this paper where the incident medium is elastic, A_x is zero everywhere. This enables elastic layers to be interbedded with absorbing media.

Extension of the Haskell-Thompson Formulation for Layered Media

The following development follows closely that of Haskell (1953, 1962). However, displacement potentials are used here. Referring to Figure 1 for coordinate reference, we can write the solutions to equation (7) in the usual form

$$\bar{\phi} = [A_p \exp(iK_{Pz}Z) + B_p \exp(-iK_{Pz}Z)]\exp(-iK_{Px}X)$$

$$\bar{\psi} = \bar{\psi}_y = [A_S \exp(iK_{Sz}Z) + B_S \exp(-iK_{Sz}Z)]\exp(-iK_{Sx}X) \tag{17}$$

where A, B are complex and in general frequency-dependent amplitudes. From equation (10)

$$K_z = P_z - iA_z; \quad K_x = P_x - iA_x.$$

In the simple case we are considering (incident elastic wave) we have $A_x \equiv 0$, and from the boundary conditions A_x must be zero everywhere. Thus K_x remains a real quantity. If the incident medium were anelastic, the incident attenuation direction would have to be specified along with the propagation direction, and then A_z in each layer would adjust itself to be consistent with a continuous A_x and a specified $K^2_{P,S}$ for that layer (see equation 14). Choosing A_P and A_S as upgoing potentials (negative z direction) we can write for each layer

$$K_z = \text{principal value } (K^2 - K_x^2)^{1/2}. \tag{18}$$

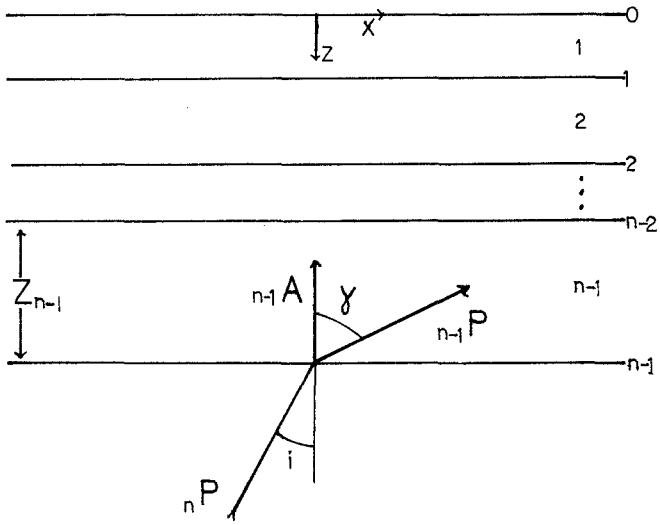

FIG. 1. The problem is uniquely specified given V_p, V_s, Q_P, Q_S, ρ, and Z for each layer and given ${}_nA_{P,S}$ (incident P- or S-wave potential amplitude) in the elastic half-space. For an anelastic half-space, the direction of the incident-wave attenuation vector must also be specified.

Using equations (2), (3), (6), (17), the displacements and stresses for layer m can be put in the following matrix form

$$\begin{bmatrix} u \\ w \\ P_{zx} \\ P_{zz} \end{bmatrix}_m = \begin{bmatrix} -iK_{Px}C_P & K_{Sz}S_S & K_{Px}S_P & -iK_{Sz}C_S \\ -K_{Pz}S_P & -iK_{Sx}C_S & iK_{Pz}C_P & K_{Sx}S_S \\ i2\bar{\mu}K_{Px}K_{Pz}S_P & -\bar{\mu}\Omega C_S & 2\bar{\mu}K_{Pz}K_{Px}C_P & -i\bar{\mu}\Omega S_S \\ \bar{\mu}\Omega C_P & i2\bar{\mu}K_{Sz}K_{Px}S_S & i\bar{\mu}\Omega S_P & 2\bar{\mu}K_{Sz}K_{Sx}C_S \end{bmatrix}_m \times \begin{bmatrix} A_P + B_P \\ A_S + B_S \\ A_P - B_P \\ A_S - B_S \end{bmatrix}_m$$

where

$$C_P = \text{Cos}\,(K_{Pz}Z_m) \qquad C_S = \text{Cos}\,(K_{Sz}Z_m)$$

$$S_P = \text{Sin}\,(K_{Pz}Z_m) \qquad S_S = \text{Sin}\,(K_{Sz}Z_m).$$

$$\Omega = K_{Px}^2 - K_{Sz}^2$$

This result (which is equivalent to equation (3–20) of Grant and West, 1965) can be conveniently written as

$$X_m = D_m(Z_m)C_m. \tag{19}$$

Thus we see that Z_m (layer thickness) is the phase factor which propagates the potentials across the mth layer and that D_m may be thought of as a form of propagator matrix with C_m the coefficient matrix. With this in mind and with the idea of eliminating C_m we can write (Haskell, 1953)

$$X_{m-1} = D_m(0)C_m; \qquad C_m = D_m^{-1}(0)X_{m-1}. \tag{20}$$

Then applying the usual boundary conditions

$$\begin{aligned} X_m &= (D_m(Z_m)D_m^{-1}(0))(D_{m-1}(Z_{m-1})D_{m-1}^{-1}(0))X_{m-2} \\ &= a_m a_{m-1} \dots a_1 X_0. \end{aligned} \tag{21}$$

and for $n-1$ layers where layer n is an elastic half-space and interface 0 is a free surface

$$\begin{aligned} C_n &= D_n^{-1}(0)a_{n-1}a_{n-2}\dots a_1 X_0 \\ &= JX_0 \end{aligned} \tag{22}$$

with the following matrix elements.

$$(-{}_mK_S^2)D_m(0)^{-1} = \begin{bmatrix} -2iK_{Px} & 0 & 0 & 1/\bar{\mu} \\ 0 & -i2K_{Px} & -1/\bar{\mu} & 0 \\ 0 & -i\Omega/K_{Pz} & -K_{Px}/(\bar{\mu}K_{Pz}) & 0 \\ i\Omega/K_{Sz} & 0 & 0 & -K_{Px}/(\bar{\mu}K_{Sz}) \end{bmatrix}_m \tag{23}$$

$$X_0 = \begin{bmatrix} u_0 \\ w_0 \\ 0 \\ 0 \end{bmatrix} \qquad C_n = \begin{bmatrix} A_P + B_P \\ A_S + B_S \\ A_P - B_P \\ A_S - B_S \end{bmatrix} \tag{24}$$

The elements of

$$(-{}_mK_S^2)a_m$$

are given by

$$\begin{aligned} a_{11} &= \Omega C_S - 2K_{Px}^2 C_P \\ a_{12} &= -iK_{Px}[2K_{Sz}S_S + (\Omega/K_{Pz})S_p] \\ a_{13} &= -\bar{\mu}^{-1}[K_{Sz}S_S + (K_{Px}^2/K_{Pz})S_p] \\ a_{14} &= -iK_{Px}\bar{\mu}^{-1}[C_P - C_S] \\ a_{21} &= iK_{Px}[2K_{Pz}S_P + (\Omega/K_{Sz})S_S] \\ a_{22} &= \Omega C_P - 2K_{Px}^2 C_S \\ a_{23} &= a_{14} \\ a_{24} &= -\bar{\mu}^{-1}[K_{Pz}S_P + (K_{Px}^2/K_{Sz})S_S] \\ a_{31} &= \bar{\mu}[4K_{Px}^2 K_{Pz}S_P + (\Omega^2/K_{Sz})S_S] \\ a_{32} &= -i2\bar{\mu}K_{Px}\Omega[C_P - C_S] \end{aligned}$$

$$a_{33}=a_{11}$$

$$a_{34}=a_{21}$$

$$a_{41}=a_{32}$$

$$a_{42}=\bar{\mu}[4K_{Px}^2K_{Sz}S_S+(\Omega^2/K_{Pz})S_P]$$

$$a_{43}=a_{12}$$

$$a_{44}=a_{22}.$$

C_n therefore becomes the input matrix and choosing $A_{P,S}$ in the upgoing $(-z)$ direction and considering incident P, we can invert equation (22) to give the surface displacements u_0 and w_0 in terms of the incident potential $({}_nA_p), K_x$, and the layering.

$$u_0=-2[J_{22}+J_{42}]_nA_p/R$$

$$w_0=2[J_{21}+J_{41}]_nA_p/R$$

$$R=[J_{21}+J_{41}][J_{12}+J_{32}]-[J_{22}+J_{42}][J_{11}+J_{31}]. \tag{26}$$

Applications

In order to illustrate the effects of attenuation, three models which represent soils, the crust, and the core-mantle boundary are considered. The structures are listed in Table 1. With the exception of the low-velocity layer of the upper mantle, these appear to be the three regions where nongeometrical attenuation is most pronounced and therefore may have some effect on observational interpretation. Also, knowledge of the Q structure of these regions will be valuable in interpreting materials and structure mechanisms when an acceptable theory is found relating state variables, material properties, and energy absorption.

In applying this formulation in calculating reflection and transmission coefficients, transfer ratios, synthetic seismograms, etc., some estimation must be made of the medium parameters. This usually means a frequency-independent loss and velocity which can be shown to violate causality (Futterman, 1962). However, since the frequency-dependence can be made weak over a finite frequency band, assuming a frequency-independent loss and phase velocity over the space-time dimensions considered here should not be critical.

(*a*) *Soils.* The effects of attenuation can be rather drastic in a highly dissipative material such as loosely compacted soils. The structure chosen (Table 1) is for the Richmond Field Station of the University of California, Berkeley and consists of mud deposited in San Francisco Bay. Borehole measurements of velocity and sample measurements of both velocity and density were available for this site. The Q structure represents a best guess for illustrative purposes (structure data from T. V. McEvilly, oral comm.). Figure 2 shows the vertical and horizontal displacement spectra for normally incident P and S waves, respectively. All input potentials were normalized to unity total displacement for incident $P({}_nA_P={}_nk_P{}^{-1})$ or $SV({}_nA_S={}_nk_S{}^{-1})$. The solid line is for an elastic stack while the broken line includes the effect of loss. The vertical motion is somewhat unstructured because the compressional wavelengths are greater than any of the layer thicknesses. The loss behaves as we might expect for purely homogeneous waves, mirroring the elastic behavior at a lower amplitude and becoming asymptotic to it toward low frequencies. Considering the shear spectra (Figure 2B) we begin to note some interesting effects. First, the elastic spectrum shows the characteristic peaks (shear wavelengths < layer thickness) which are

TABLE 1

PHYSICAL PARAMETERS FOR REPRESENTATIVE MODELS CONSIDERED IN NUMERICAL CALCULATIONS

V_p(km/sec)	V_s(km/sec)	ρ(cgs)	Q_P	Q_S	Z(km)
		Soil (Richmond)			
0.421	0.214	1.95	5	1	1.52×10^{-3}
0.641	0.299	1.95	10	2	1.53
1.007	0.299	1.95	10	3	1.52
1.296	0.305	2.00	20	4	1.43
1.464	0.305	2.00	20	5	2.14
1.525	0.317	2.05	20	5	1.83
0.488	0.305	1.97	20	5	2.13
1.739	0.427	2.08	50	10	3.05
1.647	0.397	2.00	50	10	3.75
1.739	0.427	2.05	50	10	1.52
1.678	0.323	1.92	20	5	3.05
1.952	0.372	1.97	50	10	2.44
1.793	0.329	1.92	20	5	4.27
2.034	0.488	2.19	100	20	3.66
1.983	0.900	2.30	∞	∞	∞
		Crust (Berkeley)			
4.2	2.4	2.1	67	30	1.4×10^{0}
6.1	3.5	2.6	100	45	8.2
7.3	4.2	3.0	180	80	12.9
7.8	4.5	3.3	∞	∞	∞
		Core-mantle Boundary			
13.63	7.30	5.60	∞	∞	∞
13.33	6.99	5.58	300	115	150
8.08	0	9.90	2500		∞

resonances associated with the total S-wave travel time (Bakun, 1971, Haskell, 1960). The total S-wave travel time of the stack is $T = 0.098$ sec and maxima and minima are expected at

$$f_{\max} = \frac{n}{4T}, n = 1, 3, 5, \ldots; \qquad f_{\min} = \frac{m}{2T}, m = 1, 2, 3, \ldots$$

$$= 2.6, 7.9, 12.7. \ldots \qquad = 5.1, 10.2, 20.3. \ldots$$

The peaks and troughs are not exact because the total stack travel-time effect is modulated by the layering. In the loss spectra we see that there is little information content at frequencies greater than about 14 Hz. The effect of attenuation is more drastic for shear waves due to the lower Q_S and the longer travel times. Also, it is important to note the slight shifting of the peaks in the case of loss. The velocities are the same in the elastic and attenuating layers and the shifting is due to the change in modulation as the loss affects the acoustic impedance.

In Figure 3 are shown the crustal transfer function ratio (w_0/u_0), the vertical spectra, and the horizontal spectra for an incident compressional wave at $i = 10°$ for the same soil structure. It is interesting to note the considerable change in the ratio for the loss. Any inversion scheme not accounting for the loss would yield a different structure. Again the shear spectrum is the controlling mechanism but in this case the large discrepancy between

the elastic and loss is largely due to the velocity anisotropy induced by the inhomogeneous waves (see equation 15).

(*b*) *The crust.* The crustal model (Table 1), excepting the Q structure, was taken from Bakun's best-fitting Berkeley crustal model (Bakun, 1970). The Q structure represents a

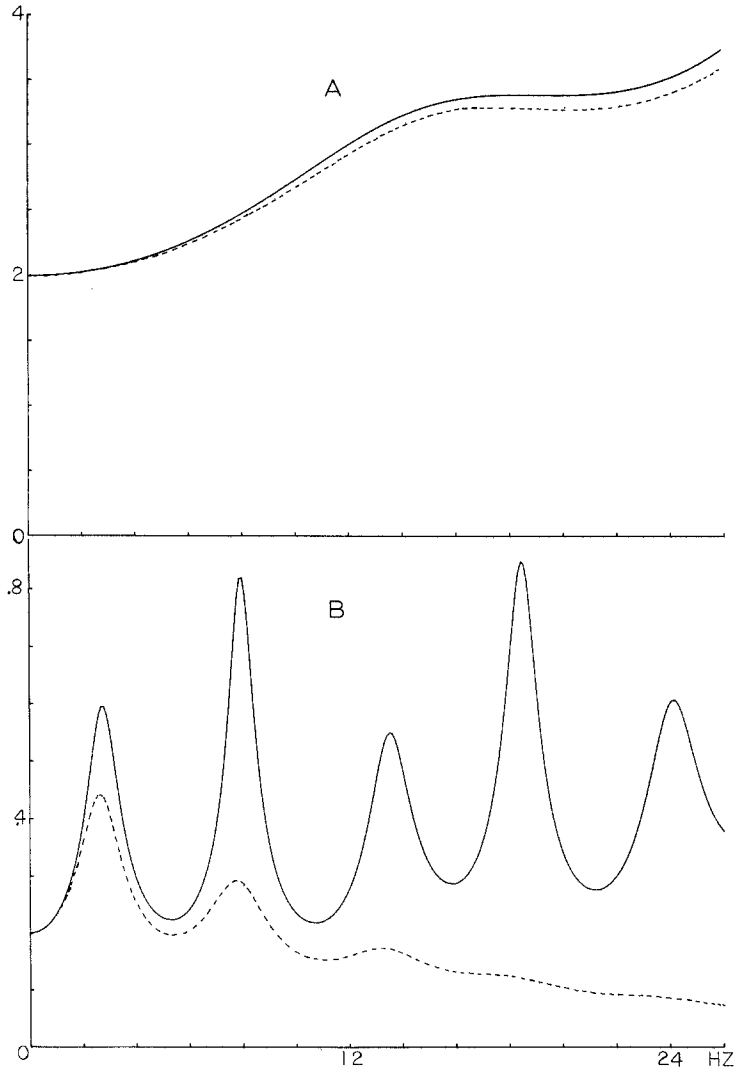

FIG. 2. Spectra of normalized surface displacements for a high-loss soil structure (Table 1). Solid lines are elastic layers, broken lines include loss. (A) Vertical displacement for incident P wave, (B) Horizontal displacement for incident S wave; both at normal incidence.

best guess for Q_S by the author based on some near-Berkeley crustal studies (Kurita, 1975, O'Neill and Healy, 1973) and the relation

$$Q_p = \tfrac{3}{4} Q_S (V_p/V_s)^2. \tag{27}$$

The transfer ratio for the crustal model for an incident compressional wave at $i = 25°$ is shown in Figure 4 along with the vertical and horizontal spectra. The transfer ratio for the elastic and loss agree well out to about 3 Hz which is high enough to resolve the structure.

The spectra of the vertical and horizontal surface displacements for the Berkeley crust have been synthesized and are shown in Figure 5, where (A) and (B) are the vertical elastic

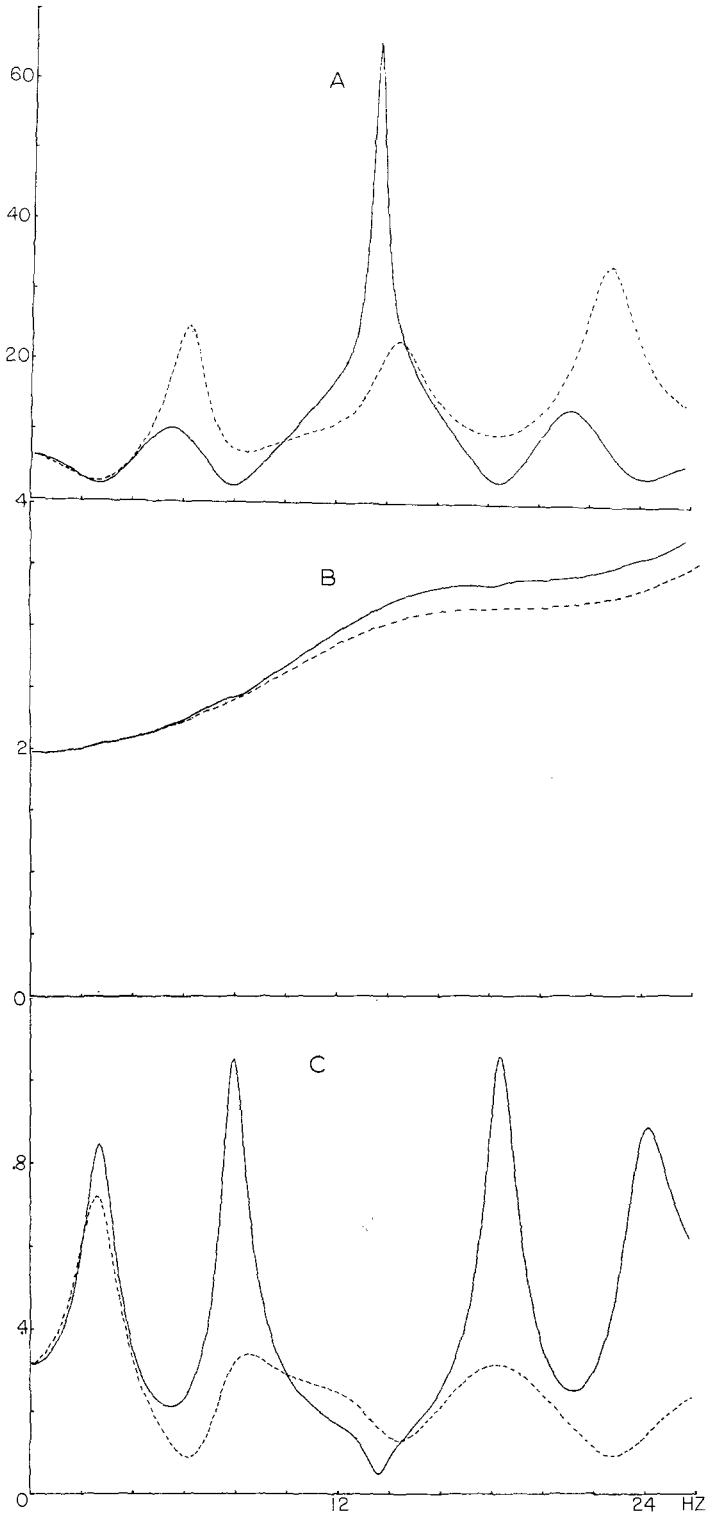

FIG. 3. Spectrum of normalized (A) crustal transfer function (w_0/u_0) (B) vertical surface displacement, (C) horizontal surface displacement for incident P wave at 10° for the Richmond structure (Table 1). Solid lines are elastic layers, broken lines include loss.

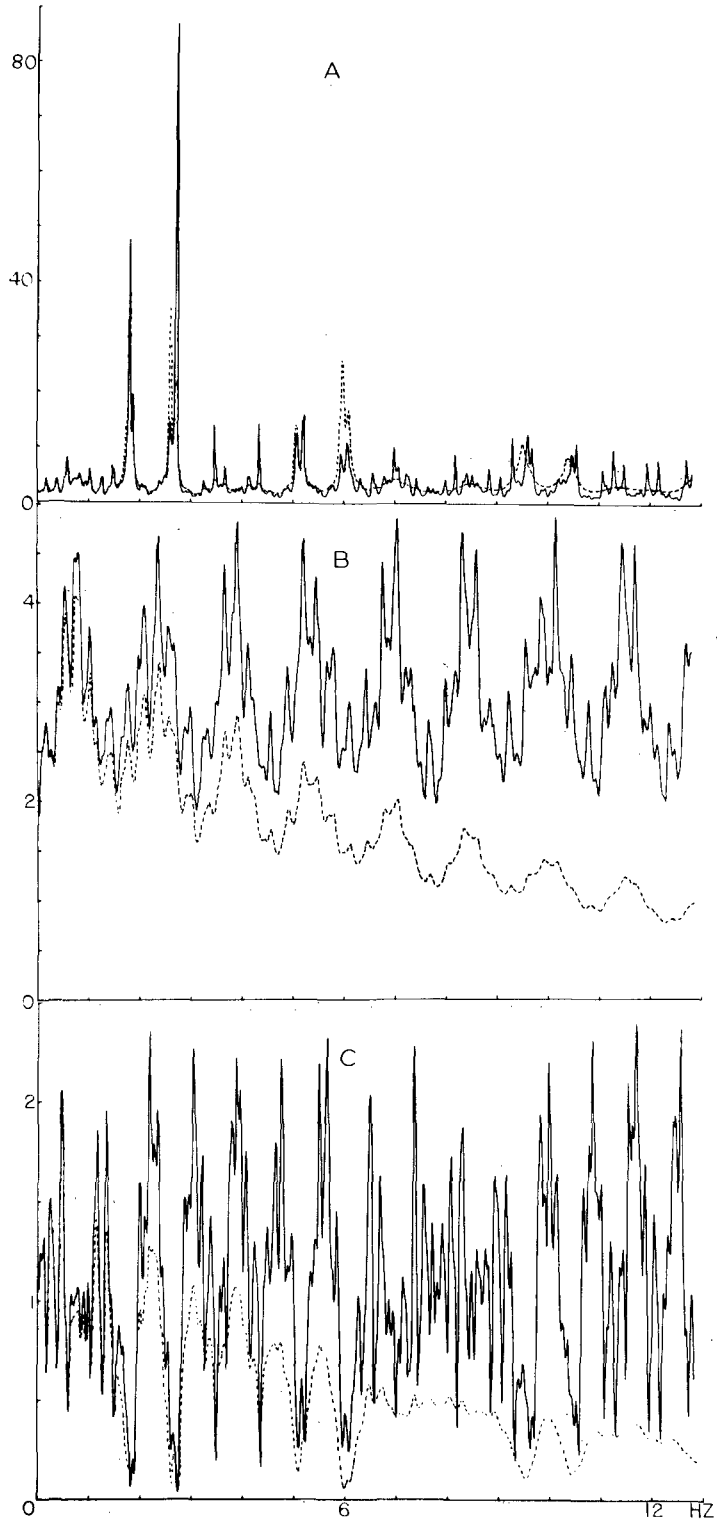

FIG. 4. Spectra of normalized (A) crustal transfer function (w_0/u_0), (B) vertical surface displacement, (C) horizontal surface displacement for incident P wave at 25° for the Berkeley crust (Table 1). Solid lines are elastic layers, broken lines include loss.

and loss while (C) and (D) represent the horizontal. The effect of the loss shows a general smoothing of the record, a decrease of the higher-order reflections, and a reduction in amplitude (vertical peak to peak by 0.7, horizontal by 0.8).

(*c*) *Core-mantle boundary.* To demonstrate the effects of loss near the core-mantle boundary on *PcP* and *PcS*, the reflection spectrum for the core-mantle boundary structure of Table 1 was synthesized. The velocities are from Bolt (1972) and the boundary layer density was derived assuming the region to be a thermal boundary layer and to consist entirely of mantle material (Glyn Jones, personal comm.). The Q_P is from Kuster (1972) while Q_S is derived from equation (27) (zero loss in bulk). An incident *P* wave is considered with $i=25°$ and the synthesis is performed for a point 70 km from the boundary layer. Figures 6 and 7 show the synthesized potential coefficients $({}_nB_p/{}_pA_p, {}_nB_S/{}_nA_p)$ for the same explosion source as the crustal seismograms. The first small pulse in Figures 6 and 7 represents reflected *P* and *SV* waves, respectively, from the abrupt transition between the lower mantle and the boundary layer. A more realistic gradient would largely eliminate this reflection. The figures then represent *PcP* and *PcS* sources to be convolved with suitable transfer functions and show the effect of attenuation on the reflected amplitudes (*PcP* zero-to-peak reduction 0.8, *PcS* 0.6). The effect on the wave forms seems to be small at this angle of incidence for such low *Q* values and indicates that a considerable amount of attenuation is possible in the boundary layer and still be unobservable.

Appendix

To consider a fluid layer ($\bar{\mu}=0$) the matrix $D_m(Z_m)$ (equation 19) must be modified due to the overspecified boundary conditions at a solid-fluid interface. Using a development similar to Teng (1967) $D_m(Z_m)$ for a fluid layer becomes

$$\begin{bmatrix} 0 & 0 & 0 & 1 \\ -k_{P_z}S_P & 0 & ik_{P_z}C_P & 0 \\ 0 & 1 & 0 & 0 \\ -\rho\omega^2 C_P & 0 & -i\rho\omega^2 S_P & 0 \end{bmatrix}_m$$

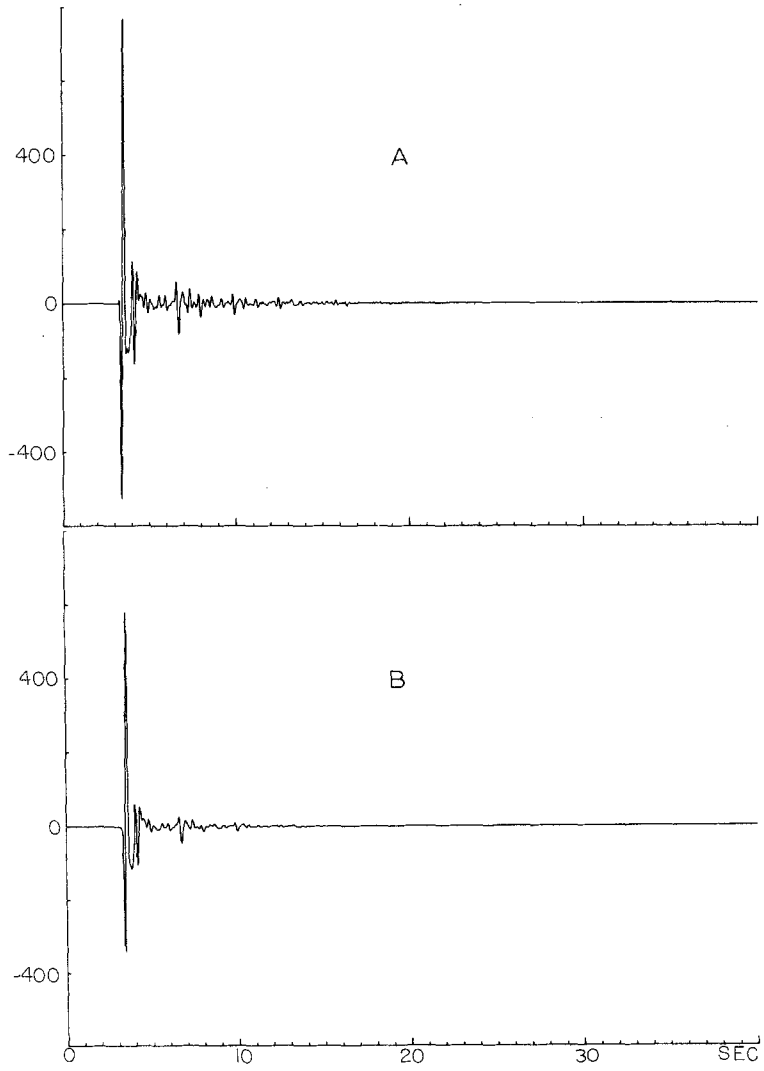

FIG. 5, A AND B.

FIG. 5. Synthetic seismograms for the Berkeley crust. (A) and (B) are vertical motion (positive down) for the elastic and loss cases, respectively, which were synthesized from the spectra in Figure 4B. (C) and (D) are horizontal motion for the elastic and loss cases, respectively, which were synthesized from the spectra in Figure 4C. All were convolved with an explosion source function appropriate for BOXCAR (Helmberger and Harkrider, 1972), a Benioff short-period instrument, and a low-pass filter with a corner frequency at 5 Hz.

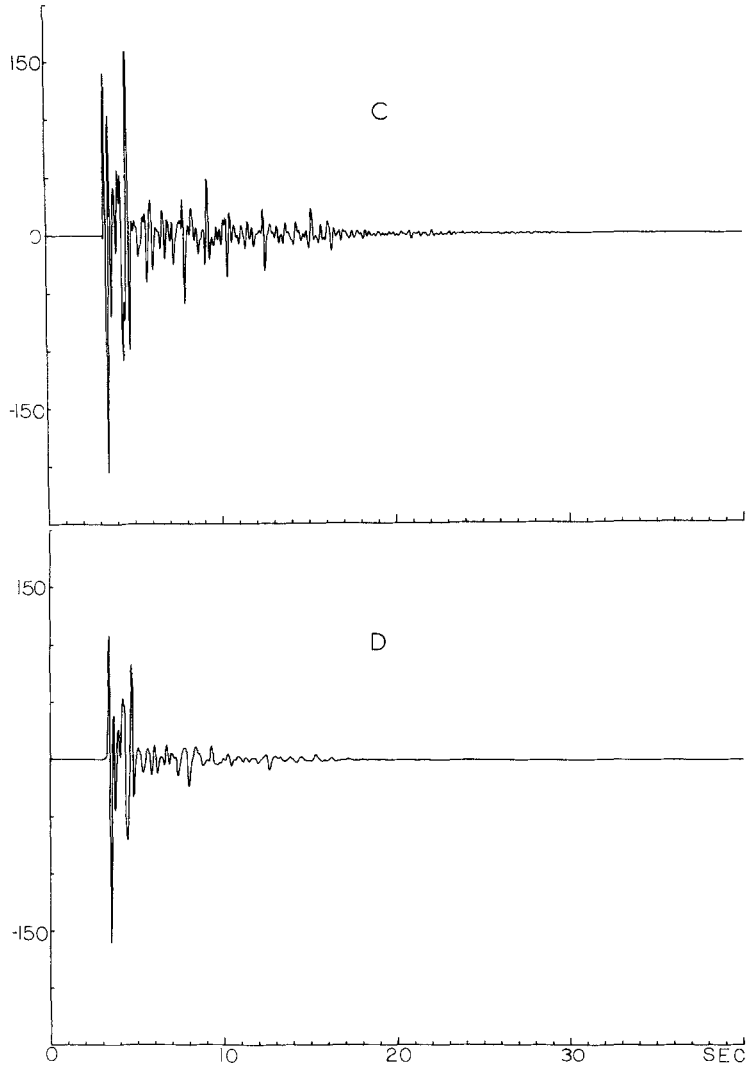

FIG. 5, C AND D.

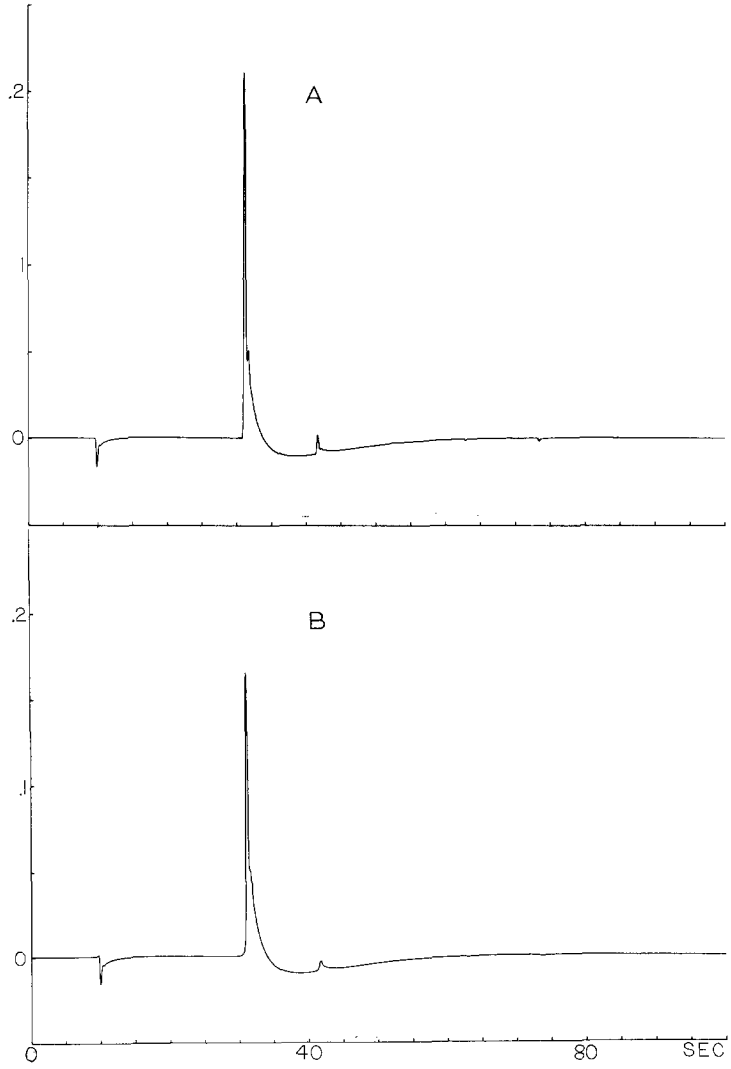

FIG. 6. Synthesized reflected *P* potential coefficient for incident *P* wave on core-mantle boundary structure of Table 1. The frequency interval was 0.01 Hz with 512 sample points. All spectra were filtered with a low-pass causal filter with corner frequency at 2.0 Hz. (A) elastic, (B) loss.

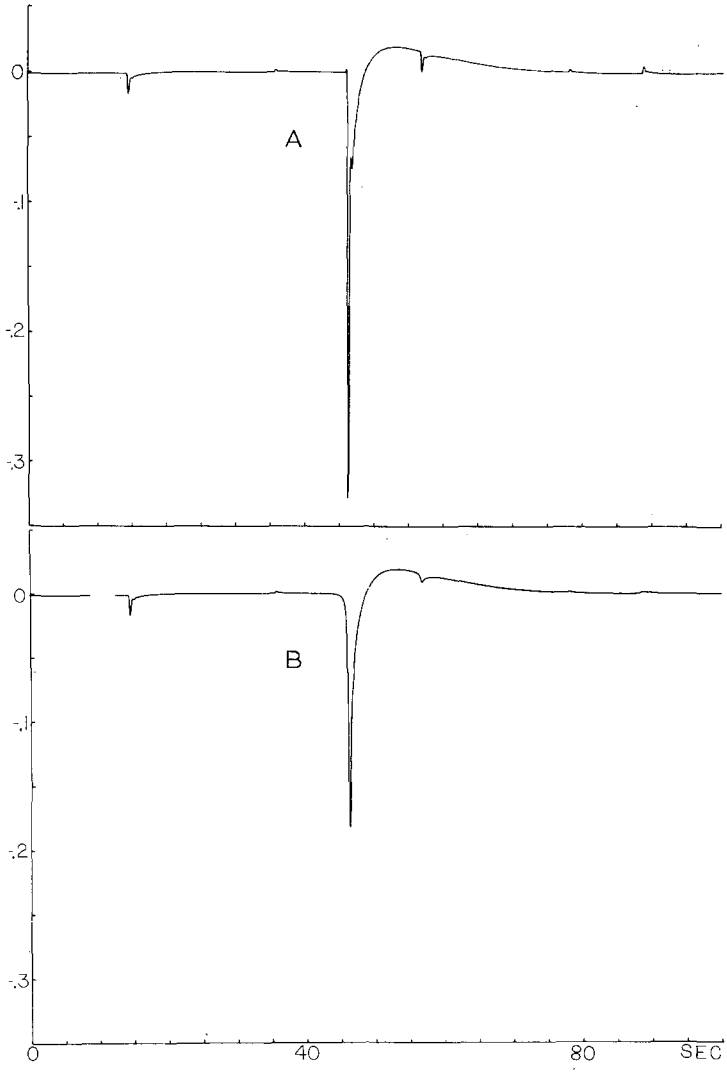

FIG. 7. Synthesized reflected S potential coefficient for incident P wave on core-mantle boundary structure of Table 1. The frequency interval was 0.01 Hz with 512 sample points. All spectra were filtered with a low-pass causal filter with corner frequency at 2.0 Hz. (A) elastic, (B) loss.

ACKNOWLEDGMENT

The author is indebted to Lane Johnson and T. V. McEvilly for suggesting the problem and for helpful comments. This research was supported by the Advanced Research Projects Agency of the Department of Defense and was monitored by the Air Force Office of Scientific Research under Grant AFOSR–73–2563.

REFERENCES

Bakun, W. H. (1970). Body-wave spectra and crustal structure: an application to the San Francisco Bay region, *Ph.D. Thesis*, University of California, Berkeley, 124 pp.

Bakun, W. H. (1971). Crustal model parameters from P-wave spectra, *Bull. Seism. Soc. Am.* **61**, 913–935.

Bolt, B. A. (1972). The density distribution near the base of the mantle and near the earth's center, *Phys. Earth Planet. Interiors*, **5**, 301–311.

Borcherdt, R. D. (1971). Inhomogeneous body and surface plane waves in a generalized viscoelastic half-space, *Ph.D. Thesis*, University of California, Berkeley, 308 pp.

Borcherdt, R. D. (1973). Energy and plane waves in linear viscoelastic media, *J. Geophys. Res.* **78,** 2442–2453.
Buchen, P. W. (1971). Plane waves in linear viscoelastic media, *Geophys. J.* **23,** 531–542.
Cooper, H. F., Jr. (1967). Reflection and transmission of oblique plane waves at a plane interface between viscoelastic media, *J. Acoust. Soc. Am.* **42,** 1064–1069.
Futterman, W. I. (1962). Dispersive body waves, *J. Geophys. Res.* **67,** 5279–5291.
Grant, F. S. and G. West (1965). *Interpretation Theory in Applied Geophysics*, McGraw-Hill, New York.
Gurtin, M. E. and E. Sternberg (1962). On the linear theory of viscoelasticity, *Arch. Ration. Mech. Anal.* **11,** 291–356.
Haskell, N. A. (1953). Dispersion of surface waves in multilayered media, *Bull. Seism. Soc. Am.* **43,** 17–34.
Haskell, N. A. (1960). Crustal reflections of plane *SH* waves, *J. Geophys. Res.* **65,** 4147–4150.
Haskell, N. A. (1962). Crustal reflection of plane *P* and *SV* waves, *J. Geophys. Res.* **67,** 4751–4767.
Helmberger, D. V. and D. G. Harkrider (1972). Seismic source descriptions of underground explosions and a depth discriminate, *Geophys. J.* **31,** 45–66.
Knopoff, L. (1964). Q, *Rev. Geophys.* **2,** 625–660.
Kanai, K. (1950). The effect of solid viscosity of surface layer on the earthquake movements, *Bull. Earthquake Res. Inst., Tokyo Univ.* **28,** 31–35.
Kurita, T. (1975). Attenuation of shear waves along the San Andreas fault zone in central California, *Bull. Seism. Soc. Am.* **65,** 277–292.
Kuster, G. T. (1972). Seismic phase propagation in two-phase media and its application to the earth's interior, *Ph.D. Thesis*, Massachusetts Institute of Technology, June.
Lockett, F. J. (1962). The reflection and refraction of waves at an interface between viscoelastic media, *J. Mech. Phys. Solids* **10,** 53 64.
O'Neill, M. E. and J. H. Healy (1973). Determination of source parameters of small earthquakes from *P*-wave rise time, *Bull. Seism. Soc. Am.* **63,** 599–614.
Teng, Ta-Yiang (1967). Reflection and transmission from a plane-layered core-mantle boundary, *Bull. Seism. Soc. Am.* **3,** 477–499.

Department of Geology and Geophysics
University of California
Berkeley, California 94720

Manuscript received November 13, 1975